Mars Entry Instrumentation Flight Data and Mars 2020 Entry Environments

Todd R. White[1], Milad Mahzari[1], Ruth A. Miller[2], Chun Y. Tang[3], Josh Monk[4], Jose A. Santos[4]
NASA Ames Research Center, Moffett Field, California 94035
Christopher D. Karlgaard[5]
Analytical Mechanics Associates Inc., Hampton, Virginia, 23666
Hannah S. Alpert[6]
Analytical Mechanics Associates Inc. at NASA Ames Research Center, Moffett Field, California 94035
Henry S. Wright[7], Chris Kuhl[8]
NASA Langley Research Center, Hampton, Virginia, 23681

On February 18th, 2021, the Mars 2020 entry vehicle delivered the Perseverance rover to the surface of Mars. The entry vehicle carried a set of instrumentation installed on the heatshield and backshell to measure aerodynamic and aerothermal performance, named the Mars Entry, Descent, and Landing Instrumentation 2. This set of instrumentation included pressure transducers, thermocouples, heatflux sensors, and a radiometer, as well as a dedicated sensor support electronics system. All MEDLI2 hardware operated as expected during cruise and entry. MEDLI2 sensors gathered accurate pressure measurements in hypersonic through supersonic regimes to reconstruct vehicle attitude and atmospheric profiles. MEDLI2 on the heatshield sensors indicated that surface temperatures, caused by turbulent heating beginning 70 seconds after entry, remained at or below 1430° C, while heatshield bondline temperatures rose less than 45° C. Backshell surface TPS temperatures peaked at 630° C, which was caused primarily by radiative heating measured by several separate sensors. The MEDLI2 temperature and pressure measurements enabled further detailed characterization of the Mars 2020 entry performance, and the flight dataset will provide a wealth of information for the EDL community and future mission designers.

Acronyms and Nomenclature

EI	=	Entry Interface
MEADS	=	MEDLI2 Entry Atmospheric Data System
MEDLI	=	Mars Entry, Descent, and Landing Instrumentation
MEDLI2	=	Mars Entry, Descent, and Landing Instrumentation 2
MISP	=	MEDLI2 Instrumented Sensor Plug
MPB	=	MEDLI2 Pressure Backshell
MPH	=	MEDLI2 Pressure Heatshield
MSL	=	Mars Science Laboratory Mission
MTB	=	MEDLI2 Thermal Backshell
MTH	=	MEDLI2 Thermal Heatshield
PICA	=	Phenolic Impregnated Carbon Ablator
SLA	=	Super Lightweight Ablator
SC	=	Spacecraft Coordinates
SSE	=	Sensor Support Electronics

[1] Senior Research Scientist, Entry Systems and Vehicle Development Branch, AIAA member.
[2] Aerospace Engineer, Entry Systems and Vehicle Development Branch, AIAA member.
[3] Senior Research Scientist, Aerothermodynamics Branch, AIAA member.
[4] Aerospace Engineer, Thermal Protection Materials Branch, AIAA member.
[5] Supervising Engineer, Associate Fellow AIAA.
[6] Systems Engineer, Entry Systems and Vehicle Engineering Branch, AIAA member.
[7] Aerospace Engineer, Space Technology and Exploration Directorate, AIAA member.
[8] Aerospace Engineer, Atmospheric Flight and Entry Systems Branch, AIAA member.

I. Introduction

The Mars 2020 Perseverance rover entered Mars' atmosphere on February 18th, 2021. The rover was protected during entry by an aeroshell that included a sensor suite to observe the entry event external surface pressures, near-surface thermal protection system (TPS) temperatures, and backshell radiative and convective heating. This sensor suite was the Mars Entry, Descent, and Landing Instrumentation 2 (MEDLI2) system [1]. MEDLI2 was derived from the successful Mars Science Laboratory Entry, Descent, and Landing Instrumentation (MEDLI), which was flown as part of the Mars Science Laboratory (MSL) aeroshell in 2012 [2]. MEDLI2 instrumentation improved on MEDLI by incorporating sensors with greater range and area coverage. MEDLI2 included new heatshield sensors to measure pressure during the supersonic portion of the entry phase. MEDLI2 also included new backshell sensors to measure the heating, pressure, and TPS response on the wake side of the entry vehicle. Finally, MEDLI2 expanded coverage of heatshield thermal measurements to better detect the onset and extent of heatshield flow transition. Figure 1 shows the MEDLI2 sensors on heatshield and backshell, prior to aeroshell integration around the Perseverance rover.

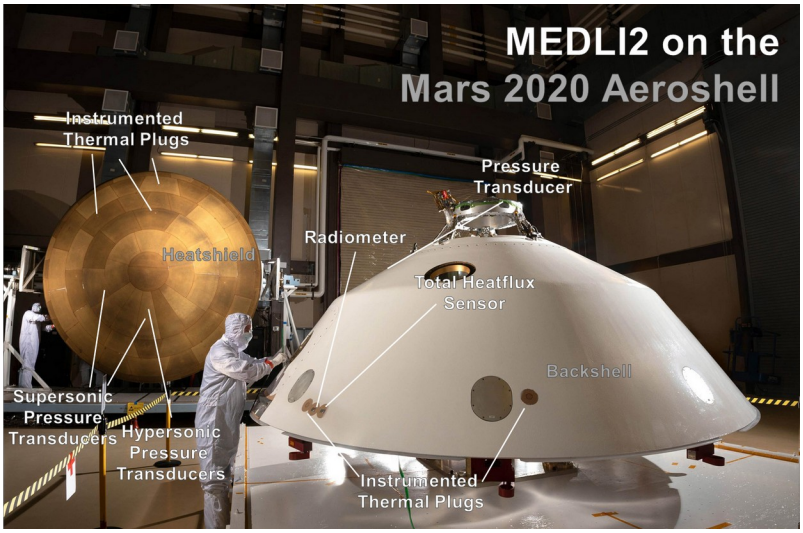

Figure 1 Mars 2020 Aeroshell with MEDLI2 Sensors

The MEDLI2 project was responsible for developing and delivering the MEDLI2 system, including all sensors, intra-instrument harnessing, and avionics. Following the successful entry of the Mars 2020 aeroshell and MEDLI2 operations, the MEDLI2 team, comprised of engineers and researchers primarily at NASA Langley (LaRC) and Ames (ARC), began assessing the flight data.

This paper is one of several papers on the MEDLI2 team's initial assessment of the returned flight data; it should be read in concert with papers that more fully describe the flight mechanics trajectory and atmospheric reconstruction [3], and aerothermal [4, 5, 6] and TPS analysis [7, 8]. The paper is focused primarily on the engineering level data returned by MEDLI2, and is organized by sensor hardware and location. The paper begins with a description of the MEDLI2 hardware, Mars 2020 operations, followed by pressure and thermal sensor sections. The paper closes with observations for future mission designers and EDL modelers.

II. MEDLI2 System Description

The MEDLI2 system was comprised of three main hardware components. The first was the pressure measurement system, MEDLI2 Entry Atmospheric Data System, or MEADS. The second was a thermal measurement system, MISP, or MEDLI2 Instrumented Sensor Plug. Both MEADS and MISP directly interfaced with the third component, the Sensor Support Electronics (SSE) and intra-instrument harnesses. The locations of the MISP and MEADS components on the heatshield and backshell are shown in Figure 2 below. MISP sensors are marked as MTH or MTB (MEDLI2 Thermal on Heatshield or Backshell) whereas MEADS sensors are marked as MPH or MPB (MEDLI2 Pressure on Heatshield or Backshell). The Mars 2020 aeroshell was a 4.5m 70° sphere-cone, and the mission flew a guided entry with a nominal angle of attack of -16° during entry. Flying at angle of

attack shifted the stagnation point away from the geometric apex (at X_{sc} = 0, Y_{sc} = 0, Z_{sc} = 2327 mm) on to the windside (X_{sc} = 1000 mm, Y_{sc} = 0 mm).

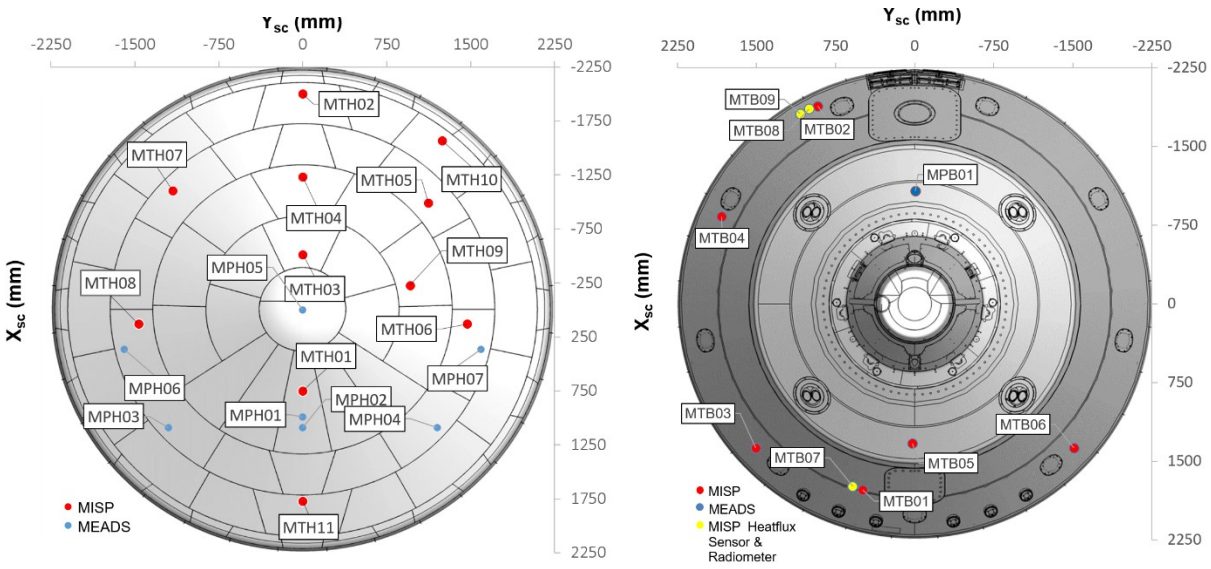

Figure 2 MEDLI2 Sensor Locations on the Mars 2020 heatshield (left) and backshell (right)

The main goals of the MEADS pressure system were to record and measure pressure during the hypersonic and supersonic flight regimes to enable reconstruction of vehicle attitude, atmospheric profile, winds, and overall aerodynamic performance. This was accomplished by three separate sensor types, across the heatshield and backshell, with ranges set based on expected pressures. The heatshield included a single hypersonic-ranged pressure transducer placed at the stagnation point (maximum range of 35 kPa), and six supersonic ranged transducers (maximum range of ~ 8 kPa). The backshell included a single low-pressure transducer on the detached leeward side, set to measure much lower (350 Pa) pressures. Figure 3 shows examples of each of the pressure transducer body types.

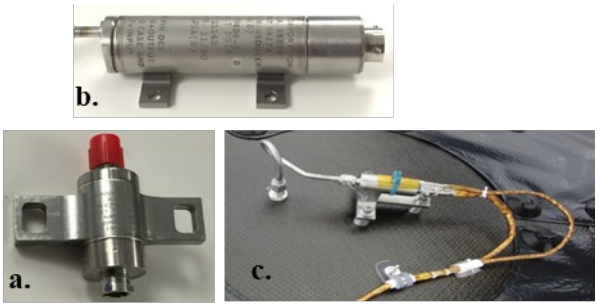

Figure 3 MEADS Pressure Instrumentation: a. Supersonic, b. Backshell, and c. Hypersonic Transducers

The main goals of the MISP thermal system were to characterize heating on the heatshield and backshell during hypersonic entry. The thermal system consisted of a series of heatshield and backshell thermocouple plugs and three direct heatflux sensing elements on the backshell. Figure 4 shows each type of heatshield and backshell MISP sensor prior to installation. On the heatshield, there were eleven PICA plugs, instrumented with in-depth and near-surface thermocouples. After the heatshield MISP TC plugs were installed, the Mars 2020 heatshield was sprayed with a light coat of NuSil CV1144-0 for dust control. This NuSil coating has been studied and shown to inhibit the normal recession of PICA in oxidizing environments, and to lower surface temperatures relative to un-coated PICA [9].

On the backshell, there were six SLA-561V plugs with near-surface thermocouples. Additionally, there were three direct heatflux-sensing instruments on the backshell: two heatflux sensors on opposing sides of the vehicle, as well as one radiometer. The backshell MISP sensors were installed after thermal control paint was applied. Each

sensor was in the middle of a large (~23 cm diameter) standoff distance, to minimize any effects of coatings on the sensors.

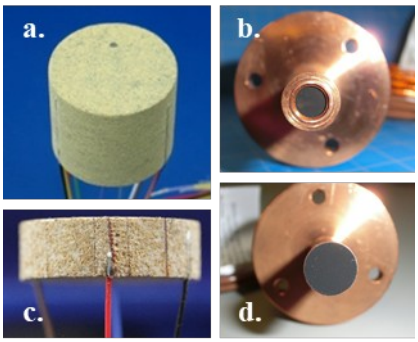

Figure 4 MISP Thermal Instrumentation Prior to Installation: a. PICA plug, b. Radiometer, c. SLA-561V plug, d. Heatflux Sensor

MISP and MEADS sensors were connected to the SSE. The SSE was a high-accuracy multiplexing system that provided an analog interface with the thermal and pressure sensors (Figure 5), and a digital interface with the Mars 2020 Descent Stage Power and Analog Module (DPAM). The MEDLI2 SSE also performed on-board averaging of the pressure transducers to reduce signal noise.

Figure 5 MEDLI2 Sensor Support Electronics

The SSE was housed on the inside of the Mars 2020 heatshield, and all readings from MEDLI2 sensors ceased at heatshield ejection soon after main chute deployment. The MEDLI2 SSE was powered on exo-atmospherically, five hours prior to entry, and it continually polled all MEDLI2 sensor channels until it was powered off just before heatshield separation. The Mars 2020 rover recorded MEDLI2 data from the SSE in a ring buffer, saving the final 20 minutes of sensor data. These 20 minutes of data included events such as cruise stage separation, entry, peak heating, deceleration, and parachute deployment, as shown in Figure 6.

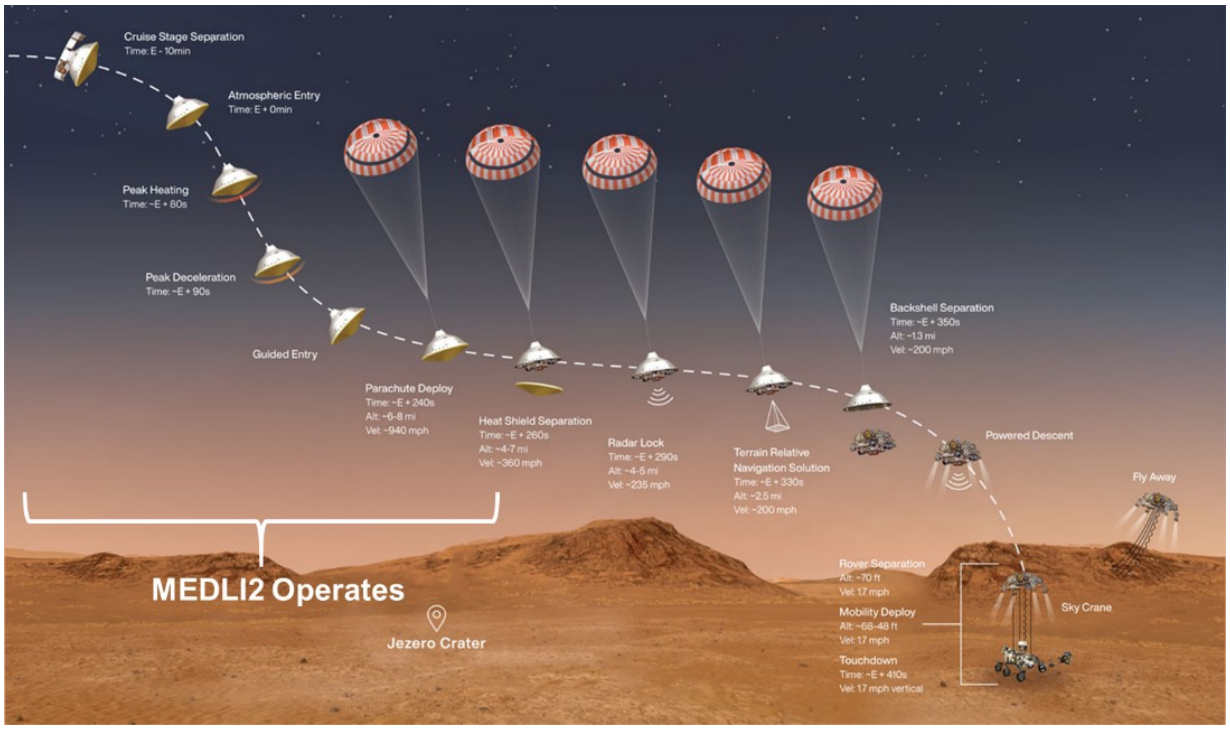

Figure 6 Mars 2020 Entry, Descent, and Landing Timeline

III. MEDLI2 Flight Data

A subset of the MEDLI2 data channels were returned as part of a Real-Time Data Product (RTDP), with all channels down-sampled to 1 Hz. These channels were selected in case the full dataset could not be retrieved, and to provide insight into the performance of the Mars 2020 entry vehicle in the unlikely event of a problem during or after EDL. The channels and the reason for selection are summarized in Table 1.

Table 1 MEDLI2 RTDP Channels

RTDP Priority	Name
Hypersonic Stagnation Pressure	MPH01
Supersonic Stagnation Pressure	MPH02
Stagnation Point Heating	MTH01-1
	MTH02-1
Turbulent Heating	MTH03-1
	MTH02-3
Turbulent Heating TPS response	MTH03-3
	MTH05-1
Symmetric Acreage Heating	MTH07-1
Backshell Pressure	MPB01
	MTB01-1
Backshell TPS Response	MTB02-1
	MTB07
Backshell Heating	MTB09

The full MEDLI2 flight data was telemetered to earth three days after landing. Upon receipt, the flight data was converted from raw signal counts into mV signals, and cross checked several times, before being converted to engineering units (e.g. Kelvin, Pascal) via calibration. The full set of science channels are described in Table 2, and the EDL-relevant portion of this data extends from Entry Interface Point (EI) through MEDLI2 shutdown. Table 2 lists the heatshield channels first, followed by backshell channels.

Table 2 MEDLI2 Science Channels

Name	Type	Rate (Hz)	Installed Location X_{sc}, Y_{sc}, Z_{sc} (mm)	Serial Number	Notes
MPH01	Hypersonic Pressure Transducer	8, 1	1004.7, -0.3, 2034.4		MEDLI spare hypersonic transducer, Strain-gage based
MPH02	Supersonic Pressure Transducer	8, 1	1089, 0.2, 2003.7	016	Piezo Resistive Transducer with internal temperature sensor
MPH03	Supersonic Pressure Transducer	8, 1	1092.4, -1200.4, 1809.3	025	Piezo Resistive Transducer with internal temperature sensor
MPH04	Supersonic Pressure Transducer	8, 1	1092.1, 1199.9, 1808.9	022	Piezo Resistive Transducer with internal temperature sensor
MPH05	Supersonic Pressure Transducer	8, 1	-0.2, -0.3, 2327.6	038	Piezo Resistive Transducer with internal temperature sensor
MPH06	Supersonic Pressure Transducer	8, 1	365.2, -1593.1, 1804.8	010	Piezo Resistive Transducer with internal temperature sensor
MPH07	Supersonic Pressure Transducer	8, 1	364.8, 1592.9, 1804.1	020	Piezo Resistive Transducer with internal temperature sensor
MTH01	3-TC PICA Plug	8, 4, 1	748.9, 0.3, 2127.7	43037-29	Type R TC at 1.98mm, Type K at 5.12 and 11.43mm
MTH02	3-TC PICA Plug	8, 4, 1	-1879, 0.9, 1716.4	43037-31	Type R TC at 1.95mm, Type K at 5.10 and 11.51mm
MTH03	3-TC PICA Plug	8, 4, 1	-515.2, 0.3, 2212.5	43037-39	Type R TC at 1.92mm, Type K at 5.16 and 11.52mm
MTH04	1-TC PICA Plug	8	-1232, 0.9, 1951.6	43037-15	Type K TC at 2.57mm
MTH05	1-TC PICA Plug	8	-989.7, 1122, 1855.7	43037-21	Type K TC at 2.59mm
MTH06	1-TC PICA Plug	8	128.4, 1469.4, 1863.4	43037-08	Type K TC at 2.58mm
MTH07	1-TC PICA Plug	8	-1104.4, -1163.6, 1816.4	43037-25	Type K TC at 2.58mm
MTH08	1-TC PICA Plug	8	129.2, -1468.9, 1863.6	43037-09	Type K TC at 2.58mm
MTH09	1-TC PICA Plug	8	-228.2, 960.2, 2041.1	43037-11	Type K TC at 2.59mm
MTH10	1-TC PICA Plug	8	-1432.5, 1217.5, 1716	43037-27	Type K TC at 2.59mm
MTH11	1-TC PICA Plug	8	1773.1, -0.1, 1754.9	43037-03	Type K TC at 2.58mm
MPB01	Low Pressure Transducer	8, 1	-1078.7, -0.3, 200.3	39026	Variable Reluctance Transducer, with external RTD for temperature
MTB01	2-TC SLA-561V Plug	8, 4	1773.4, 491.2, 901.4	44031-19	Type K TCs at 2.56mm and 6.37mm
MTB02	1-TC SLA-561V Plug	8	-1882.4, 921.4, 1237.9	44031-06	Type K TC at 2.61mm
MTB03	1-TC SLA-561V Plug	8	1376.9, 1509.6, 1170.6	44031-01	Type K TC at 2.61mm
MTB04	1-TC SLA-561V Plug	8	-830.4, 1835.8, 1130.2	44031-09	Type K TC at 2.62mm
MTB05	1-TC SLA-561V Plug	8	1325.6, 20.5, 351.2	44031-10	Type K TC at 2.62mm
MTB06	1-TC SLA-561V Plug	8	1374.4, -1510.2, 1169.2	44031-05	Type K TC at 2.61mm
MTB07	Heatflux Sensor	16, 1	1743.2, 586.6, 899	205138	Schmidt-Boelter Gauge with surface TC
MTB08	Heatflux Sensor	16, 1	-1809.1, 1083.5, 1254.3	205137	Schmidt-Boelter Gauge with surface TC
MTB09	Radiometer	16, 1	-1854.9, 1003.7, 1254.2	2051323	Sapphire window over Schmidt-Boelter with surface TC

A. Overall MEDLI2 performance during Entry

MEDLI2 sensors and electronics operated with no dropouts or un-expected signal noise. The MEDLI2 team conducted two cruise checkouts, in the months before entry, which showed the MEDLI2 SSE operated as expected. During these checkouts, the team measured pressure transducer in-flight zeros, and assessed temperature stability of the SSE and sensors. A similar process was conducted in the hours leading up to atmospheric entry. All indications were that the SSE remained within the designed and expected environments during entry, and performed as expected. The paper turns now to the pressure measurements.

B. MEADS Surface Pressure Flight Data

The in-flight pressure data from the hypersonic (MPH01), supersonic (MPH02-07), and backshell (MPB01) transducers are shown in Figure 7. These MEADS measurements, combined with data from the Mars Climate Sounder (MCS), onboard Inertial Measurement Unit (IMU), and Mars Environmental Dynamics Analyzer (MEDA) were used in a Kalman filter to reconstruct the atmosphere and entry vehicle attitude [3].

The pressure histories are the result of processing the raw sensor mV to kPa; this included removal of spikes due to pyro-shock events, incorporating temperature-dependent sensor calibration, and applying additional corrections for transducer hysteresis during the dynamic pressure pulse. Due to schedule constraints, the dynamic pressure pulse

tests were conducted after entry and on flight spares. These hysteresis effects were incorporated for each sensor in the Kalman filtering, which provided the final processing of the pressure transducer data shown in this paper.

The heatshield and backshell pressure signals had high signal to noise, with the hypersonic and backshell pressure transducers staying within the full measurement range at all times. The supersonic pressure transducers saturated during the hypersonic pressure pulse as expected. The backshell pressure picked up events such as reaction control system thruster firings (130-150s), and events leading up to and including parachute deployment. The MEDLI2 team developed a polynomial fit for base drag for use in flight mechanics simulations; the form of the fit is similar to the Pathfinder-based Mitcheltree correlation [10].

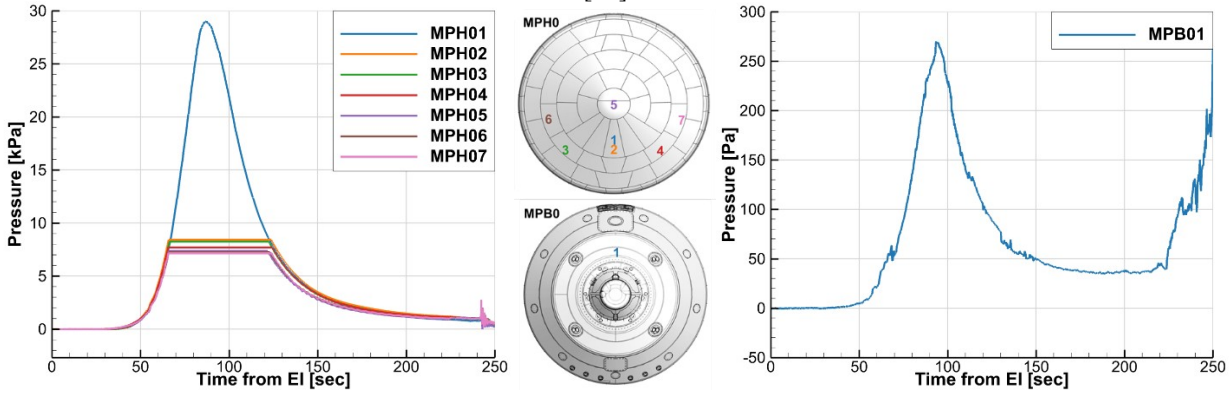

Figure 7 Heatshield and Backshell Pressure as measured during entry

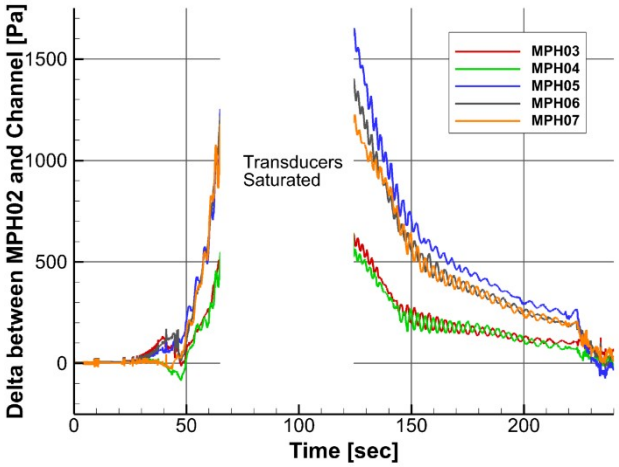

Figure 8 Supersonic Transducers: Pressure Deltas from Stagnation

The pressure transducer magnitudes and relative values were consistent with pre-entry CFD predictions. Figure 8 shows the difference between the supersonic pressure transducer (MPH02) and the other supersonic transducers. Each pair of symmetric sensors (MPH03-MPH04 and MPH06-MPH07) recorded similar pressure magnitudes, and in-phase oscillations that corresponded with vehicle banking maneuvers. The more windward pair (MPH03-MPH04) saw higher pressures than the more leeward pair (MPH06-MPH07) or that of the geometric apex (MPH05). More detail on treatment of flight pressure data and the resulting reconstructed trajectory and atmosphere can be found in Reference 3.

C. MISP Forebody Temperature Flight Data and Observations

The focus now shifts from pressure measurements to heatshield temperature measurements. The heatshield temperature measurements from MISP (MTH01-MTH11) thermocouples are shown in Figure 9. Thermocouples are labelled as either near-surface (-1), or in-depth (-2 and -3). Three of the near-surface thermocouples in the heatshield MISP plugs were slightly closer to the outer mold line (OML), specifically MTH01-1, MTH02-1, and MTH03-1,

thus MTH02-1, and MTH03-1 temperatures are higher, and out-of-family with the other near-surface (-1) temperature measurements in Figure 9.

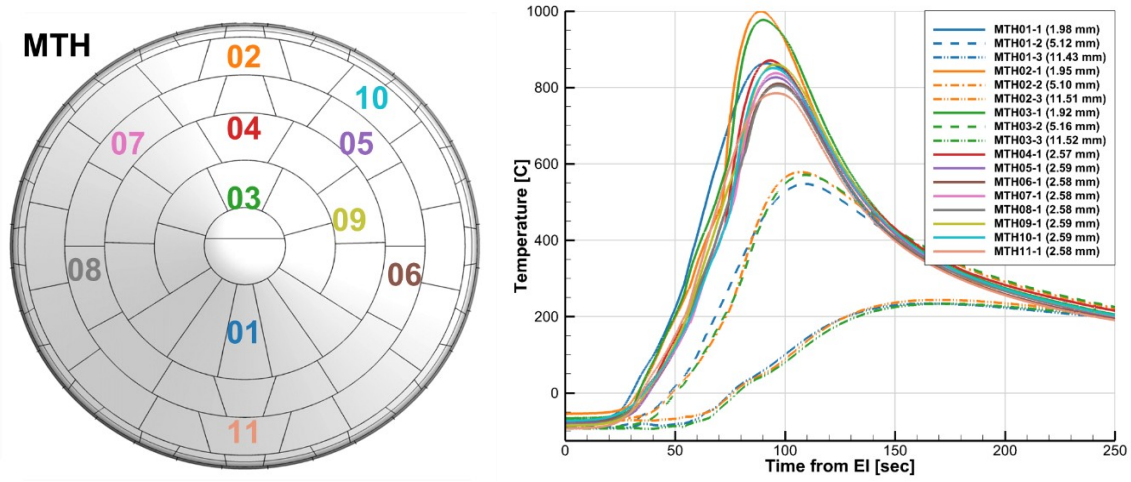

Figure 9 Heatshield Temperatures measured during entry measured by MISP

The heatshield TC signals all had high signal to noise, with peak temperatures remaining just under 1000° C, and all TCs remained within their measurement ranges, with no burn-out or melting that is characteristic of TPS recession past the TC wiring depth. This indicates there was little to no recession (< 1.9mm) on the heatshield. The slope change in nine of the eleven near-surface thermocouples starting at 70 seconds was attributed to transition from laminar to turbulent flow [5, 8], similar to what MSL/MEDLI observed [1].

Heating across the heatshield appeared to be symmetric as well. Examining the symmetric MISP pairs MTH08 and MTH06, as well as MTH07 and MTH10, revealed the near-surface temperatures were within 5° C of each other prior to flowfield transition, and within 20° C of each other through the rest of the entry pulse, as shown in Figure 10.

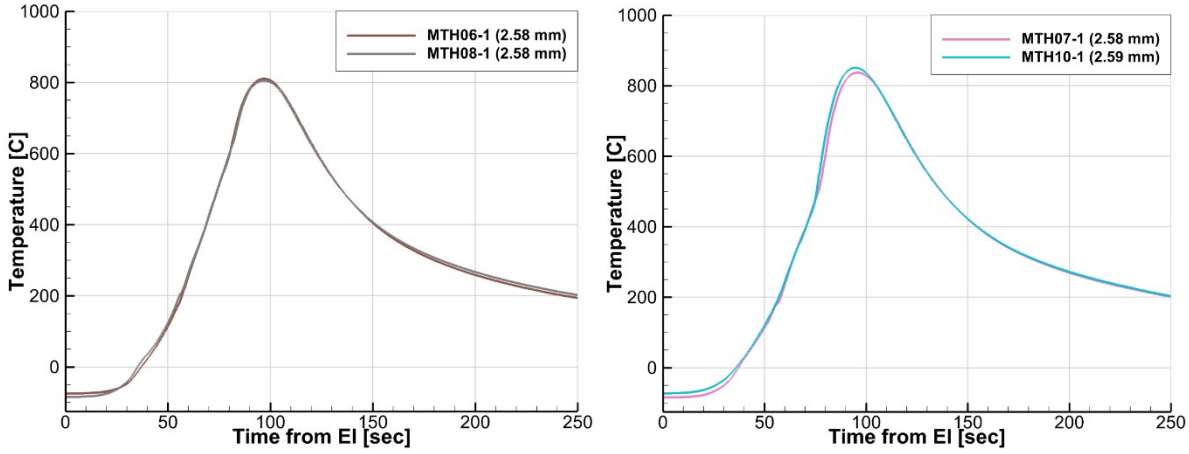

Figure 10 Comparison of near-surface temperature in symmetric heatshield TCs

The follow-on detailed interpretation of flight data and model comparison for the heatshield TC data is described in greater detail by Monk [7], Alpert [8], Tang [5], and Edquist [4]. This paper will address some of the important aspects of that work here, in particular the results of two different approaches for interpreting and using TPS temperature measurements.

The first approach was *direct analysis*, wherein the flight temperatures were directly compared to predicted temperatures, typically from 1-D ablator model. For direct analysis, the simulation boundary conditions can come from either from computational fluid dynamics [4, 5], or they may be from the actual flight data itself, a so-called "TC driver" analysis. For this direct analysis, an ablator model is required [7] and the MEDLI2 project invested in

pre-flight experimental characterizations of the specific plug TPS. The MEDLI2 team then used these characterizations to refine the ablator models, starting from the model used for TPS sizing and design by the Mars 2020 project. This refined model was necessary, because while MEDLI2 TPS plug materials were within the performance specification for PICA, they were different enough that using the standard design model would lead to additional errors. Specifically, the design ablator model for PICA included higher virgin and char conductivity than the MEDLI2 measurements on witness coupons. To validate the MEDLI2 models, the team made numerous comparisons with arc jet test TC measurements, where the refined MEDLI2 ablator models were compared to the TC measurements. The MEDLI2 refined ablator models improved agreement, particularly when performing "TC driver" analysis across multiple TCs (e.g. top, or TC1 driving bottom, or TC3) for all rounds of arc jet testing. Using the MEDLI2 specific model significantly reduced the over-prediction of in-depth temperatures from TC1 to TC3, by as much as 45° C [7].

The second approach for interpreting the internal TC measurements of TPS temperature was *inverse estimation*, [8, 11]. Here, instead of comparing measured and predicted internal temperatures, the temperature history at one location (just below the surface) was used to estimate the heating and temperature history *at the surface.* Much like the direct analysis described previously, inverse estimation also required an ablator response model. This analysis relied on the refined response model developed for direct analysis, as well as the uncertainties in the main parameters of this model. For MEDLI2, the ablator experimental characterizations and their uncertainties allowed uncertainties to be defined around important parameters such as density and thermal conductivity.

One major difficulty in the MEDLI2 direct and inverse analysis was the thin layer of NuSil coating on top of each of the heatshield MISP plugs. As of late 2021, a validated model is in development, but is not sufficiently mature for inclusion in flight analysis. For the MEDLI2 reconstruction efforts to date, analysis proceeded using the PICA model for un-coated PICA with no recession, to mimic the primary effect of NuSil on PICA behavior.

Using these inverse estimation results and assumptions, the MEDLI2 team estimated that heatshield external surface temperatures peaked at 1427° C, with peak heating (at MISP locations) of 79 W/cm^2. Inverse estimation also confirmed timing of transition; heatshield laminar to turbulent flowfield transition occurred generally as expected, starting at 70 seconds from EI at the leeside shoulder MTH02 and to the most outboard forward locations (MTH06 and MTH08) 8-11 seconds later.

Figure 11 shows the combination of the actual flight TC data, alongside the inverse estimated surface temperature estimates. Surface temperature estimates begin at entry interface and terminate at 150 seconds, after which inverse solutions become less accurate due to the low heating. The inverse estimation technique sometimes amplified small changes in internal temperatures, which leads to oscillations in reconstructed surface temperatures, particularly around 50-55 seconds in MTH04, MTH06, and MTH07.

Finally, the results of the direct analysis for bondline temperature histories are shown in Figure 12 and summarized in Table 3. Table 3 also describes the thermal mass of the substructure below the PICA plugs. MEDLI2 sensors were installed over several different substructure layouts, and locations with greater thermal mass were predicted to have smaller temperature increases. Across all MEDLI2 heatshield sensor locations, the bondline temperature increased by less than 45° C.

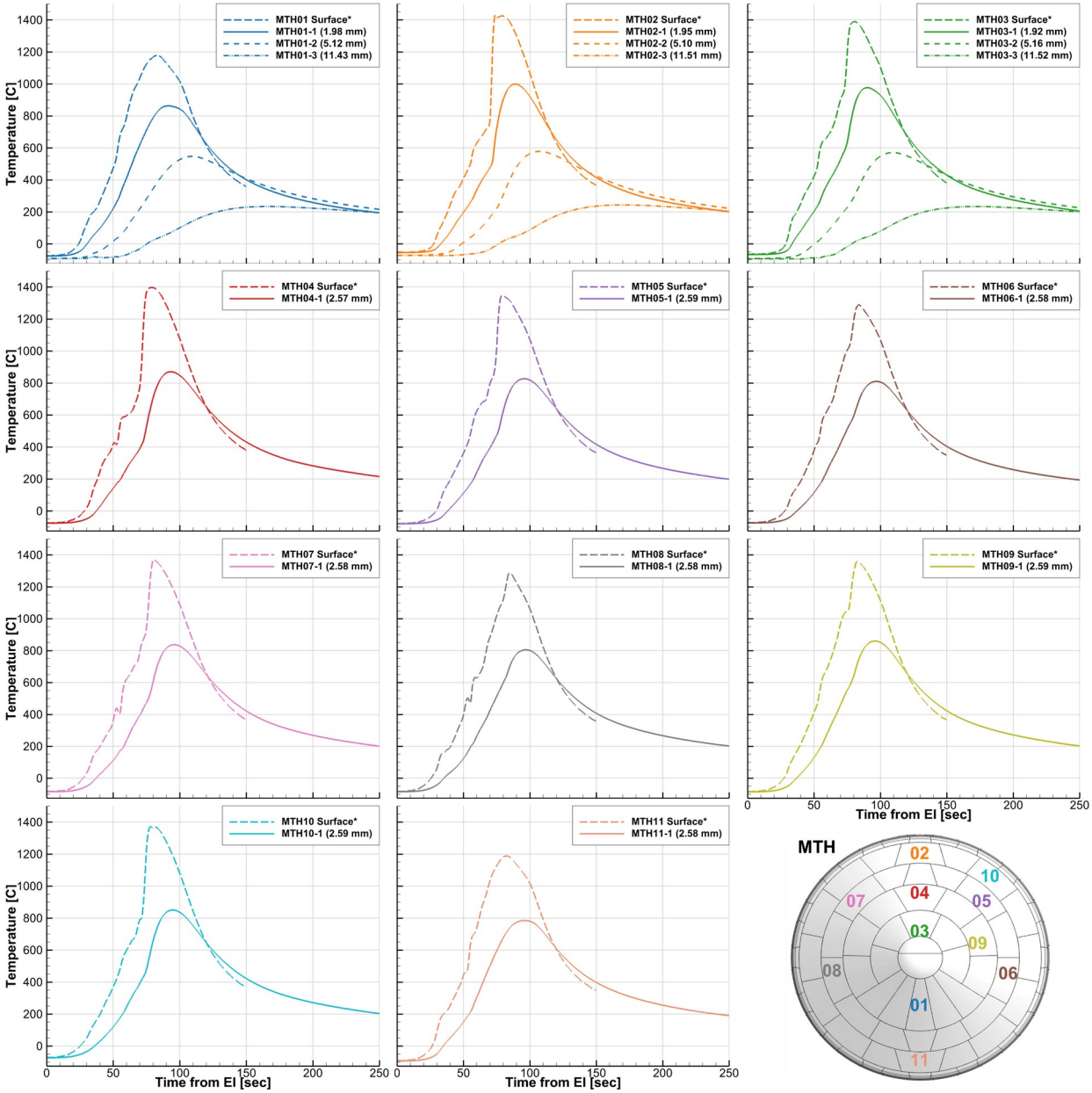

Figure 11 All MISP Heatshield Measured Temperatures and *Estimated Surface Temperatures

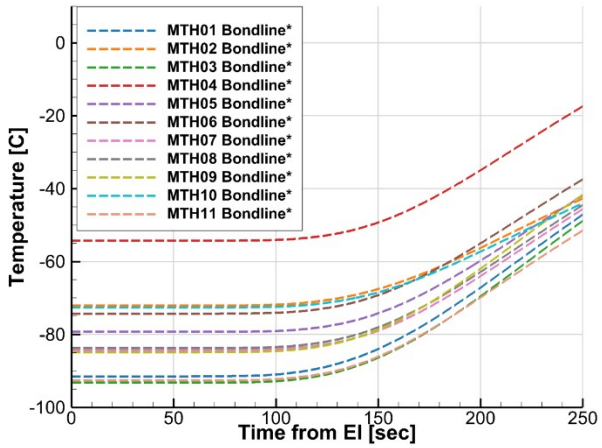

Figure 12 *Estimated Bondline Temperatures at Heatshield MISP locations from Direct Analysis

Table 3 Heatshield Bondline Temperature Summary

Location	Substructure Areal Thermal Mass (J/m^2-K)	Heatload (J/cm^2)	Peak Heatrate (W/cm^2)	Initial Temperature (deg C)	Final Temperature (deg C)	EI to HS Sep Increase (deg C)
MTH01	3048	1296.5	30.4	-91.5	-47.1	44.4
MTH02	5860	1672.5	68.4	-72.0	-42.6	29.4
MTH03	3048	1584.7	54.5	-93.2	-48.6	44.5
MTH04	3371	1593.1	57.7	-54.3	-17.3	37.0
MTH05	3371	1398	52.8	-79.3	-41.7	37.5
MTH06	3371	1294.7	42.4	-74.3	-37.3	37.0
MTH07	3371	1426.4	54.3	-84.3	-45.4	38.8
MTH08	3371	1276.8	41.9	-83.7	-44.3	39.4
MTH09	3048	1510.3	49.2	-84.8	-41.4	43.4
MTH10	5860	1495.7	56.6	-72.6	-43.9	28.7
MTH11	3868	1276.9	31.7	-92.6	-51.3	41.3

D. MISP Backshell Temperature Flight Data and Observations

The focus now shifts to backshell temperature measurements. The backshell temperature measurements are shown in Figure 13. One plug (MTB01) included an in-depth TC measurement (MTB01-2). The variation in initial temperature in the backshell was noticeable, due to the much lower overall heating and orientation of the backshell relative to the sun prior to entry. At MTB02, MTB03, and MTB04 the temperature at 2.54mm was -46° C, and at MTB05 and MTB06 there was a warmer initial temperature of -29° C. MTB01 initial temperatures at 2.54mm fell in between, with a -38° C initial temperature. There was a mild thermal gradient in the TPS due to solar heating, at the second TC in MTB01 at 6.35mm was 4° cooler than at 2.54mm.

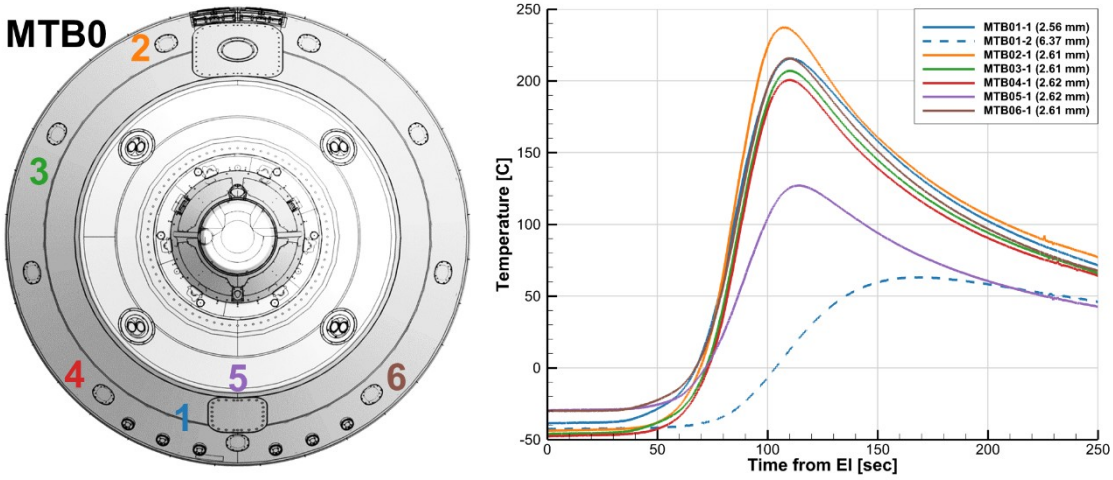

Figure 13 Backshell Temperatures measured during entry measured by MISP

During entry, the backshell sensor with the greatest temperature rise was near leeside centerline (MTB02), and the lowest temperature rise was at MTB05, on windward on centerline on the second cone. The leeside experienced higher heating than the windside (Figure 14a), and there was a trend in sensors from windside to the leeside (Figure 14b). Also, peak temperatures increase moving windside to leeside (MTB03 to MTB04, and MTB02). These trends are consistent with estimates of increasing importance of radiative heating moving from windside to leeside [12].

There were no obvious signs of rapid changes in the backshell environments, on account of laminar to turbulent flow transition at MTB01, MTB03, or MTB06 where the flow is likely attached; there was also no discernable difference between MTB03 and MTB04 to indicate major convective heating differences due to separation line movement. Measured peak backshell temperatures occur later (100s) than forebody peak temperatures (~90s), which is consistent with expectations that heatshield heating peaks earlier than backshell heating.

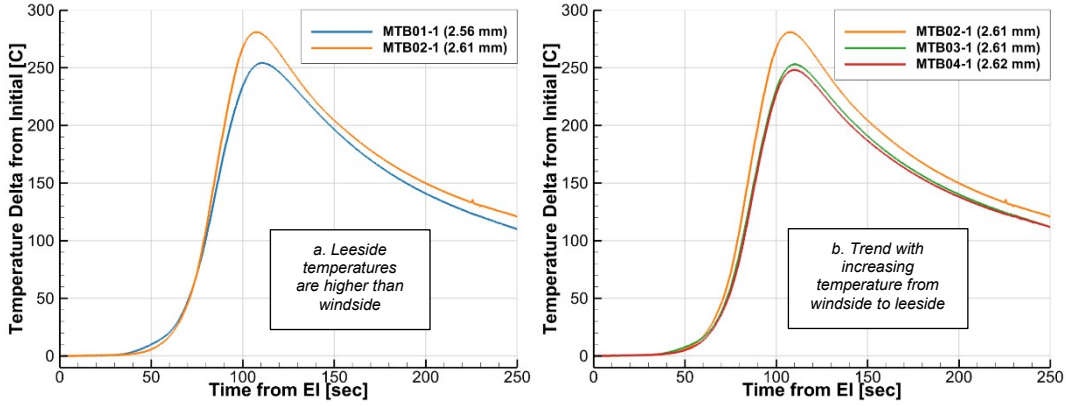

Figure 14 Comparisons of temperature rise from individual aftbody MISP channels

As with the heatshield MISP, MEDLI2 developed a refined SLA-561V ablator model to support direct [7] and inverse analysis [8] of the backshell TC data. The main refinement for the MEDLI2 SLA-561V model was removal of a conservatism in the design SLA-561V model—specifically the inclusion of pressure-dependance in the material conductivity. This refinement, combined with MEDLI2-specific adjustments to temperature-varying virgin and char conductivity (reduced by 25-45%) greatly improved ablator model comparisons to arc jet TC data.

On the backshell, there was a single location where direct analysis used flight data for a "TC driver" analysis (MTB01-2 and MTB01-2), and there the refined SLA-561V ablator model also compared well. The inverse estimation in [8] further refines much of the trends observed in the raw TC data above. The peak backshell surface temperatures stayed below 630° C, with all hot-wall heatrates at or below 4.5 W/cm^2.

Figure 15 shows the combination of the backshell flight TC data next to the inverse estimated surface temperatures. The results of direct analysis of bondline temperature histories are shown in Figure 16, and summarized in Table 4. MEDLI2 backshell sensors locations were predicted to have increased by less than 29° C.

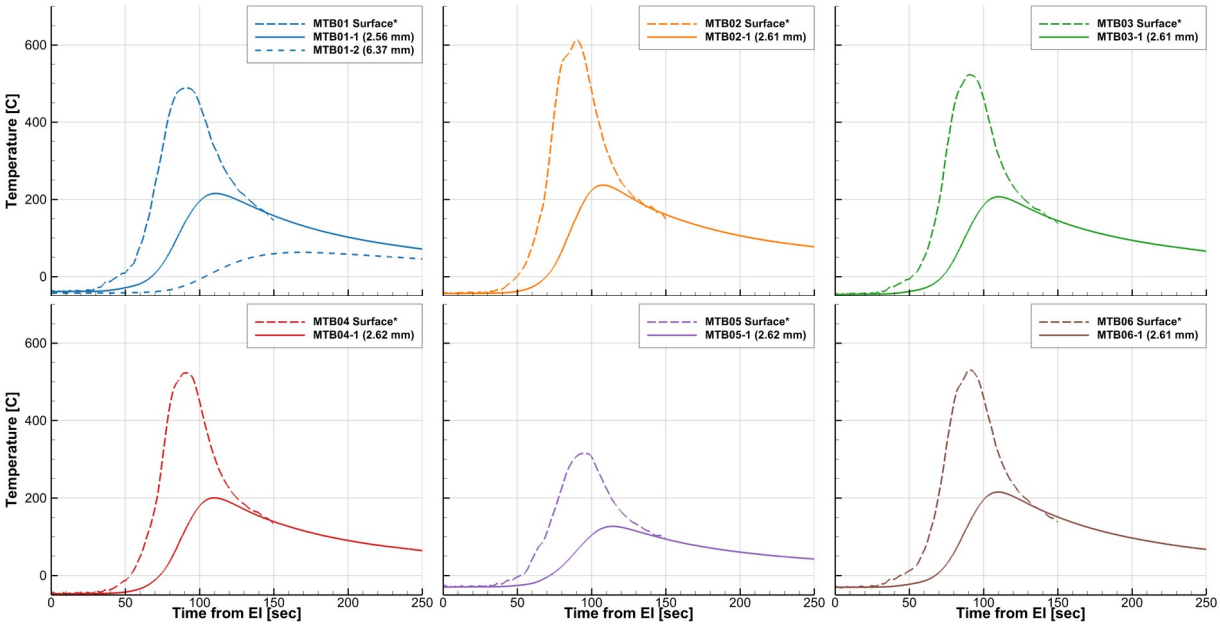

Figure 15 All MISP Backshell Measured Temperatures and *Estimated Surface Temperatures

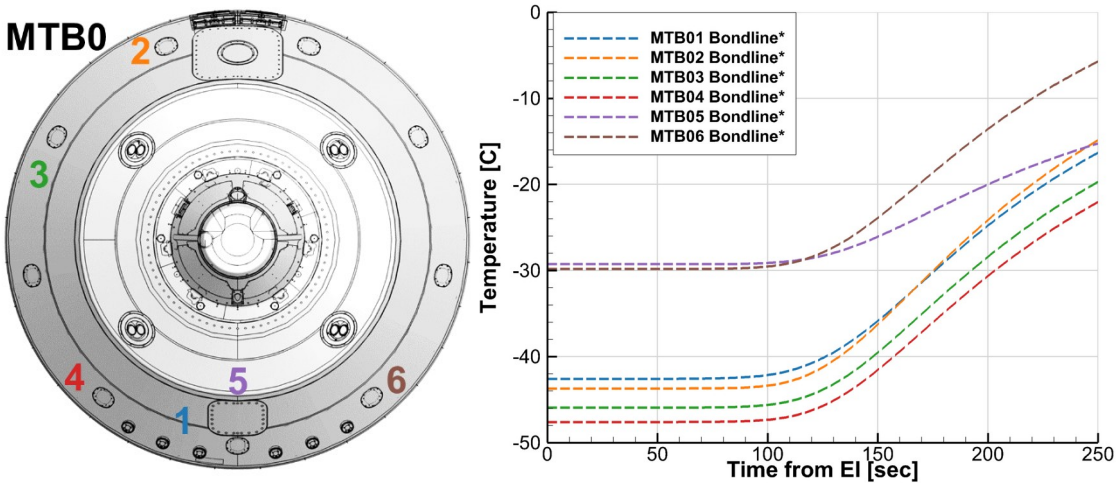

Figure 16 Bondline Temperatures at Backshell MISP locations as *estimated from TC driver simulations

Table 4 Backshell Bondline Temperature Summary

Location	Substructure Areal Thermal Mass (J/m^2-K)	Heatload (J/cm^2)	Peak Heatrate (W/cm^2)	Initial Temperature (deg C)	Final Temperature (deg C)	EI to HS Sep Increase (deg C)
MTB01	5040	109	2.95	-42.6	-16.3	26.3
MTB02	5040	138.3	4.5	-43.7	-14.8	28.9
MTB03	5040	108.4	3.31	-45.9	-19.6	26.3
MTB04	5040	103.3	3.28	-47.6	-22.0	25.6
MTB05	5363	51.7	1.38	-29.3	-15.2	14.1
MTB06	5040	108.5	3.35	-29.8	-5.7	24.2

E. MISP Backshell Direct Heatflux Flight Data

The paper turns to the other backshell thermal sensors. The heatflux gage and radiometer sensor measurements are shown in Figure 17(a), in mV (Schmidt-Boelter readings) and degrees Celsius (surface temperatures). The entry pulse was detected by all three sensors, both in the sensor mV output increases and surface temperature increases. Initial temperatures for the two leeside sensors (MTB08 and MTB09) were around -37° C, with the windside sensor cooler at -46° C. The overall sensor tips remained cold, despite the nearby TPS reaching much higher temperatures at adjacent instrumented plugs (MTB01 and MTB02).

Converting from mV output to the engineering units of interest (W/cm^2) required calibration curves, and corrections for view angle and surface coatings as described in Miller [6]. The resulting heatflux, after calibration and view factor, and other corrections are shown in Figure 17(b).

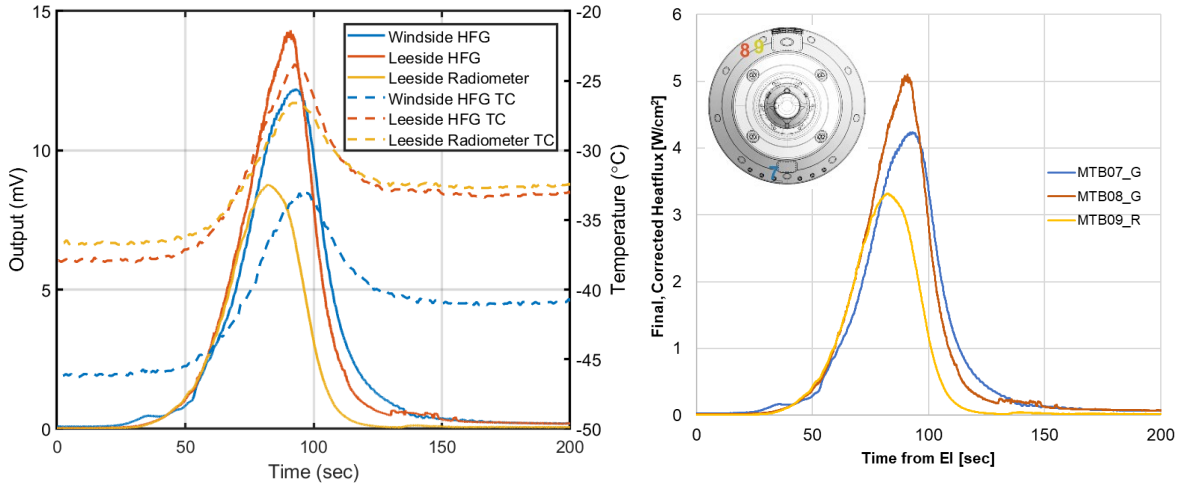

Figure 17 a. Heatflux and radiometer raw signals, tip temperatures measured during entry, and b. Heatflux values

Like the backshell TCs, the heatflux sensor measurements confirm the leeside of the backshell experienced higher peak heating than the windside. Miller also describes how the measured peak total heating on the windside and leeside of the M2020 heatshield are well predicted by current state of the art models (DPLR/NEQAIR) when tip and surrounding TPS temperatures are included in the simulations [6].

The radiometer measured backshell radiation of 3.3 W/cm^2, confirming the effect and considerable magnitude of CO_2 Mid-Wave infrared radiation as predicted and inferred from the European Schiaparelli EDL instrumentation suite [13]. The radiometer was susceptible to signal attenuation due to ablation products that can deposit on the sapphire window during entry. Therefore, the heating measured by the radiometer can be treated as a lower bound on radiation at the MTB09 sensor location. The MEDLI2 team investigated several approaches to estimate blockage that occurred during flight. One approach was to compare the radiative heatflux (MTB09) with the simulated radiative pulse, on the basis that at MTB09 most of the predicted heating was radiative, and the adjacent total heatflux sensor (MTB08) agreed with simulation results. This approach indicated the radiative heating blockage was 42-53%, with blockage increasing linearly during the entry pulse. Additional approaches included assessing

blockage in ground test experiments where radiometers were exposed to ablation products derived from arc heated TPS. At the end of such tests, the sapphire windows were extracted and measured for transmissibility. As Miller shows, the degree of blockage varied considerably in these tests, though the results bound the inferred blockage of the first approach. Therefore, there are likely to remain open questions as to the extent and effect of ablation products on the MEDLI2 radiometer regardless of future testing or modeling efforts.

Practically, however, the combination of heatflux sensor and radiometer together effectively bounded backshell radiation. The radiometer provided a lower bound of radiation (peak of 3.3 W/cm^2) at the backshell leeside shoulder because ablation products inhibit measurements of true radiation. The heatflux sensor (MTB08), which measured convective and radiative heating and is not susceptible to ablation product blockage, provided the upper bound (5.1 W/cm^2) on radiation.

IV. Implications for Future EDL Missions and Modeling

Like the MSL/MEDLI flight data before it, MEDLI2 provided a large dataset for further interpretation and entry modeling. In addition to the flight data itself, the MEDLI2 project also developed specific models which provide insight into possible improvements for modeling and mission design.

For pressure transducers, the MEDLI2 project conducted dynamic pressure testing to address the possibility that sensor signals may be altered following the hypersonic entry pulse. This testing showed the importance of hysteresis and led to updated sensor models with the NewSTEP Kalman filter. For future missions with pressure transducers, this kind of dynamic pressure pulse testing should be incorporated in sensor selection and pre-launch characterization to further reduce reconstruction uncertainty.

For TC plugs, MEDLI2 developed refined material response models for both PICA and SLA-561V. These response models (and the experiments used to develop them) were effectively a "sensor calibration" step for the combination of TC and surrounding TPS. Future instrumented EDL missions would be well served to follow the MEDLI2 approach of tracking individual plug TPS characteristics and performing material characterization tests on these specific ablators. Even with these refined models, MEDLI2 reconstruction still over-predicted deeper thermocouple temperatures when compared to arc jet and flight data; this implies there remains some inherent conservatism in these models. For the heatshield, this could likely be improved by accounting for water phase change and energy transport, as has been demonstrated by Omidy [14] for MSL/MEDLI.

For the forebody PICA plugs, the thin silicone NuSil coating motivates further research and high-fidelity ablator models; this is an active area of ongoing research at NASA through a MEDLI2 Deep Dive effort under NASA's Entry Systems Modeling project [9, 15]. This research will address how the coating alters high-temperature gas-surface interactions, and will also attempt to bound the impact of the coating given the uncertainty on the actual amount of NuSil sprayed atop the heatshield TC plugs.

For the backshell, the trio of thermal sensors and single pressure measurement may yield further information when treated together. Simple comparisons can be used to infer more details on heating, for instance between the cold-surface tip heatflux sensor measurements and the hot-wall inverse-estimated heating at adjacent TPS plugs. Development is underway as part of the MEDLI2 Deep Dive to apply Kalman Filters techniques to combine multiple backshell thermal measurements foroverall lower-uncertainty heating estimates [16]. The backshell sensors also picked up RCS thruster firings occurring at ~130-150s, which will provide an opportunity for possible validation of low dissipation time-accurate CFD [17].

From a vehicle design perspective, the MEDLI and MEDLI2 data can be combined to assess performance of the aerodynamic models used in flight mechanics simulations. The backshell pressure measurements have already been used for a refined backshell drag contribution model. Current state of the art aerothermal CFD and radiation simulations predict the MEDLI2 inverse estimated heating relative magnitudes well on the forebody and backshell [4, 5] This agreement indicates that aerothermal CFD is capturing relative heating trends well, though forebody peak heating magnitudes sometimes exceed the nominal aerothermal predictions. This indicates a continued need for aerothermal margins in design and investments in improved aerothermal and TPS modeling.

MEDLI2 data and reconstruction can be combined with MSL/MEDLI to support designing to transitional flow environments. Future M2020-class missions may incorporate flight transition timing in concert with existing transition prediction correlations [5], which may reduce peak design heatrates and integrated heatloads. Incorporating transitional environments in vehicle design may also reduce TPS mass or risk if it is combined with a tailored (non-uniform) thickness heatshield.

V. Conclusion

MEDLI2 represented NASA's most ambitious EDL instrumentation effort at Mars, to provide crucial insights into the EDL performance of the heaviest Mars lander to date. The MEDLI2 sensor suite functioned as designed, and returned valuable information on the entry pressures, temperatures, heating environments, and TPS performance. The MEDLI2 flight data enabled detailed trajectory and atmospheric reconstruction [3], as well as detailed assessments of the entry TPS [7, 8], and aerothermal [4, 5, 6] environments. The MEDLI2 flight data confirmed details of important trends in entry environments, including heatshield pressure distributions and turbulent onset, and backshell radiative heating. MEDLI2 has provided an incredibly useful engineering dataset for immediate assessment of Mars 2020 performance and will be a further resource for improving future EDL missions and modeling.

VI. Acknowledgements

The authors gratefully acknowledge the effort of the entire MEDLI2 Project team across NASA LaRC, ARC, JPL, and Lockheed Martin, and the technicians who fabricated and installed the MEDLI2 flight hardware. The authors appreciate the NASA organizations at GCD/STMD, HEOMD, and SMD that enabled the MEDLI2 project.

References

[1] Hwang, H., Bose, D., White, T., Wright, H., Schoenenberger, M., Kuhl, C., Trombetta, D., Santos, J., Oishi, T., Karlgaard, C., Kuhl, C., Mahzari, M., and Pennington, S., "Mars 2020 Entry, Descent and Landing Instrumentation (MEDLI2)," AIAA Paper 2016-3536, AIAA Thermophysics Conference, Washington, DC, June 2016. https://doi.org/10.2514/6.2016-3536

[2] Cheatwood, F. M., Bose, D., Karlgaard, C. D., Kuhl, C. A., Santos, J. A., Wright, M. J., "Mars Science Laboratory (MSL) Entry, Descent, and Landing Instrumentation (MEDLI): Complete Flight Data Set," NASA TM-2014-218533, October 2014.

[3] Karlgaard, C., Schoenenberger, M., Dutta, S., Way, D. "Mars Entry, Descent, and Landing Instrumentation 2 Trajectory, Aerodynamics, and Atmosphere Reconstruction", paper submitted to AIAA SciTech 2022, San Diego.

[4] Edquist, K., Mahzari, M., and Alpert, H., "Mars 2020 Reconstructed Aerothermal Environments and Design Margins", paper submitted to AIAA SciTech 2022, San Diego.

[5] Tang, C., Mahzari, M., Prabhu, D., Alpert, H., Cruden, B., "Mars 2020 Entry Inferred Aerothermal Environments", paper submitted to AIAA SciTech 2022, San Diego.

[6] Miller, R., Tang, C., White, T., Cruden, B., "MEDLI2: MISP Measured Backshell Aerothermal Environments", paper submitted to AIAA SciTech 2022, San Diego.

[7] Monk, J., Feldman, J., Mahzari, M., White, T., Prabhu, D., Alpert, H., "MEDLI2: Ablator Models for Flight", paper submitted to AIAA SciTech 2022, San Diego.

[8] Alpert, H., Saunders, D., Mahzari, M., Monk, J., White, T., "Inverse Estimation of Mars2020 Entry Aeroheating Environments Using MEDLI2 Flight Data", paper submitted to AIAA SciTech 2022, San Diego.

[9] Ventura Diaz, P., Meurisse, J., Brandis A. M., Bessire, B. K., Barnhardt, M., and Yoon, S., "High-Fidelity Simulations of HyMETS Arc-Jet Flows for PICA-N Modeling", AIAA 2021-1629, 2021.

[10] Dyakonov, A. A., Schoenenberger, M., and Van Norman, J. W., "Hypersonic and Supersonic Static Aerodynamics of Mars Science Laboratory Entry Vehicle," AIAA 2012-2999, 2012.

[11] Mahzari, M., Braun R., White, T., and Bose, D. "Inverse Estimation of the Mars Science Laboratory Entry Aeroheating and Heatshield Response", *Journal of Spacecraft and Rockets* Vol. 52, No. 4, July–August 2015.

[12] Brandis, A.M., Saunders, D.A., Johnston, C.O., Cruden, B.A., and White, T.R., "Radiative Heating on the After-Body of Martian Entry Vehicles," *Journal of Thermophysics and Heat Transfer*, Vol. 34, No. 1, 2020, pp. 66-77.

[13] Brandis, A.M., White, T.R., Saunders, D.A., Hill, J.P., and Johnston, C.O., "Simulation of the Schiaparelli Entry and Comparison to Aerosciences Flight Data," *Journal of Spacecraft and Rockets*, Articles in Advance, 2021.

[14] Omidy, et al. "Effects of Water Phase Change on the Material Response of Low-Density Carbon-Phenolic Ablators", Journal of Thermophysics and Heat Transfer, Vol. 30, No. 2, April–June 2016.

[15] Chen, Y., "Thermal Analysis for Phenolic Impregnated Carbon Ablator/CV-1144-0 in Hypersonic Test Environments", *Journal of Spacecraft and Rockets*, Articles in Advance, 2021.

[16] Karlgaard, C., Stoffel, T., White, T., West, T., "Data Fusion of In-Flight Aerothermodynamic Heating Measurements Using Kalman Filtering", abstract submitted for AIAA Aviation 2022 conference.

[17] Stern, E., Schwing, A., Brock, J. M., and Schoenenberger, M. "Dynamic CFD Simulations of the MEADS II Ballistic Range Test Model", AIAA 2016-3243, 2016.